Journal of Applied Polymer Science

Investigation of the Crystalline Phase Morphology of a β-Nucleated Impact Polypropylene Copolymer

Teboho S. Motsoeneng,[1] Adriaan S. Luyt,[1] Albert J. van Reenen[2]
[1]Department of Chemistry, University of the Free State (Qwaqwa Campus), Phuthaditjhaba, South Africa
[2]Department of Chemistry and Polymer Science, University of Stellenbosch, Stellenbosch, South Africa
Correspondence to: A. S. Luyt (E-mail: luytas@qwa.ufs.ac.za)

ABSTRACT: This study covers the preparation and the characterization of β-nucleated impact polypropylene copolymer (NA-IPC). Calcium stearate (CaSt), as well as pimelic (Pim) and adipic (Adi) acids, were doped into IPC as mono- or bicomponent nucleating agents (NAs) at varying mass ratios. Possible chemical interactions between the NAs and with IPC, as well as the effect of the NAs on the crystallization behavior and nonisothermal crystallization kinetics, were investigated. DSC and XRD results revealed that IPC nucleated with Pim and Pim-CaSt nucleants induced up to 90% β-crystals, whereas Adi and Adi-CaSt formed only about 17% β-crystals. This was associated with the strong nucleation efficiency of Pim. The nonisothermal crystallization kinetics showed that the crystallization of IPC and NA-IPC followed a three-dimensional growth with athermal nucleation mechanism. FTIR showed that none of the NAs chemically reacted with IPC, and the chemical structure of the polymer was thus intact during the treatment. © 2013 Wiley Periodicals, Inc. J. Appl. Polym. Sci. **2013**, *000*, 39923.

KEYWORDS: copolymers; crystallization; differential scanning calorimetry (DSC); kinetics; X-ray

Received 7 May 2013; accepted 1 September 2013
DOI: 10.1002/app.39923

INTRODUCTION

Isotactic polypropylene (iPP) is a semicrystalline commodity polymer which, by virtue of its nature, is described as a polymorphic material. In essence, it possesses several crystallographic forms, namely monoclinic (α), trigonal (β), triclinic (γ), and smectic forms. The α-modification is a thermodynamically stable and very common crystalline phase of iPP. The trigonal form is known by its metastable character and has excellent properties compared to the other crystalline phases. The triclinic phase is normally established in low-molecular-weight iPP and in propylene random copolymers under very high pressure conditions. The smectic mesophase is a middle phase between the ordered and disordered (amorphous) phases.[1–5]

The polymorphs (α, β, γ, and smectic phase) of polypropylene have a certain structural feature in common, because they share three helical (3_1) conformations in the crystal lattice structure. However, structural instability of the beta form can generate supermolecular structures (SMSs) in a certain range of crystallization temperatures. The features of the β-modification are readily affected by the crystallization conditions, the presence of inappropriate particles, and the melting history of the sample.[2,3,5,6]

Structural polymorphism of iPP is typically established in its crystalline domain, and the manipulation of the β-crystals can be easily achieved under feasible conditions, that include the addition of a selective and efficient beta inducing nucleating agent (NA), and thermal treatment through a step-by-step crystallization temperature gradient.[4] These methods can create a fair amount of β-crystals, but cannot completely eradicate the robust (α-polymorph) crystalline phase. The introduction of the NA can either further increase or decrease the amount of α-crystals, or somewhat enforce the formation of both β- and α-crystals. β-nucleation is normally disturbed by the introduction of a strong α-inducing NA, or the binary blending of iPP with another polymer component having a strong α-activity, or a preparation method which is unfavorable for β-nucleation.[3,7,8]

Although iPP is considered as a fascinating polymorphic material, it has weak impact properties, especially at lower temperatures. This can be overcome by blending iPP with an elastomeric material, or by inducing β-crystal formation in iPP which has also been found to improve the impact strength. Beta crystals decrease the stiffness the polymer, but increase the crystallization temperature. Introduction of an effective nucleant noticeably decreases spherulites size and haziness.[5,8,9]

A number of research groups investigated the effect of different NAs in iPP and in iPP-based copolymers. Generally, the nucleated iPP copolymers showed a lower extent of β

© 2013 Wiley Periodicals, Inc.

Table I. Mass Ratios of the Respective Nucleating Agents and the Total Mass of the IPC Matrix in the Blends

IPC (g)	Pimelic acid (g)	Adipic acid (g)	Calcium stearate (g)	Ratio
99.4	0.2		0.4	1 : 2
99.4		0.2	0.4	1 : 2
99.4	0.15		0.45	1 : 3
99.4		0.15	0.45	1 : 3
99.4	0.6			1 : 0
99.4		0.6		1 : 0
99.4			0.6	0 : 1

modification than iPP. It was suggested that the phase separation between the distinctive matrices would lead to inefficient β-crystal formation. The reason for this is that the NA is situated in the second polymer component, especially where both the second polymer component and the NA contain polar groups, thus thwarting the effectiveness of β-nucleation. In the case of a polyamide (PA)/iPP blend, it was found that a compatibilizer decreased the particle size of the discontinuous phase (PA), which promoted homogeneity, and enhanced β-nucleation.[10–12] When ethylene copolymers of iPP were investigated, it was found that the smaller the size of the dispersed phase, the better the impact strength.[13] In a more recent paper,[14] the authors investigated the phase morphology and toughening behavior of IPC with and without NA, prepared at different processing temperatures. Depending on the presence of a NA and/or the processing temperature, they observed three different structures: a well-defined core–shell structure, a developing multilayered structure, and an incomplete phase separation structure with interpenetrating chains.

This article reports on the nucleation efficiency (NE) and crystallization behavior of an impact polypropylene copolymer (IPC) nucleated in the presence of pimelic acid (Pim), adipic acid (Adi) and their combinations with calcium stearate (Pim-CaSt and Adi-CaSt). Differential scanning calorimetry (DSC) and X-ray diffraction (XRD) were used to determine the extent of α- and β-crystallization, and DSC was used to investigate the crystallization kinetics of the systems where the largest extent of β-crystallization was observed.

MATERIALS AND METHODS

A commercial impact polypropylene copolymer (IPC) grade (trade name CMR648) with a melt flow rate (MFR) of 8.5 g/10 min (230°C/2.16 kg) was purchased from Sasol Polymers, South Africa. It has an ethylene content ranging between 10 and 13%, a melting temperature of 163°C, and a density of 0.904 g cm^{-3}. Pimelic acid, adipic acid, and calcium stearate were supplied by Sigma–Aldrich, South Africa. A mixture of Irganox 1010 and Irgafos 168, used as antioxidant, was supplied by Sasol Ltd. *via* the University of Stellenbosch, South Africa.

Individual and compounded NAs, together with 1.5 wt % of antioxidant, were completely dissolved in a sufficiently large volume of acetone at room temperature. The total weight percentage of nucleant was kept constant at 0.6 wt %. In the case of the bicomponent nucleant, the respective nucleants were calculated in such a way that their combined weight percentage was 0.6 wt %. The mass ratios of the mono- and bicomponent NAs are shown in Table I. The pimelic and adipic acids, and the calcium stearate are, respectively, denoted by Pim, Adi, and CaSt throughout the writing of this article.

The completely dissolved nucleants (0.6 wt %) together with 1.5 wt % antioxidant were transferred into a beaker containing 99.4 g IPC pellets. The solution covered all the pellets in a beaker. Each composition was left in a fume-hood overnight to ensure the complete evaporation of acetone. The dried compositions were extruded by using a Brabender Plastograph single screw-extruder at 60 rpm screw speed. The temperature profile of the four controllable thermocouples was set to be 150, 175, 175, and 200°C from the hopper to the die. The extruded samples were cooled and pelletized. Pristine IPC with antioxidant but free from NA was also prepared using the same processing method. The granules were then placed between two pressure release hot stages at 200°C for 5 min to ensure the complete melting of the granules. The molten samples were pressed at 200°C under 50 kPa for 5 min to form 15 × 15 cm^2 square sheets. After removal from the hot press, the sheets were left at room temperature for 24 h. The films were then placed between the two cold plates of the hot press. The temperature was then gradually increased to 200°C, and the films were re-pressed for 10 min. The hydraulic pressure was then decreased to zero, while the film was left between the hot plates. The hot press was then switched off to allow the temperature to decrease until it was at ambient temperature. The samples were removed and stored for further analysis.

A Perkin Elmer Pyris-1 differential scanning calorimeter (DSC) was used in this work to quantitatively determine the amount of β-polymorph formed in nucleated IPC. The DSC was calibrated using the melting temperatures of indium and zinc, and the melting enthalpy of indium. The analyses were done under flowing nitrogen atmosphere (20 mL min^{-1}). Samples with masses between 5 and 10 mg were sealed in aluminum pans. The samples were heated from 25 to 220°C and held for 5 min to erase the thermal and mechanical history, cooled from 220 to 25°C, and reheated from 25 to 200°C at 10°C min^{-1}. Each composition was analyzed three times to confirm reproducibility. From an analysis of each set of three repeat curves, the average values and standard deviations in Table II were calculated. Nonisothermal crystallization kinetics were investigated for pure IPC, IPC/Pim-Cast (1 : 2), and IPC/Pim-Cast (1 : 3) by DSC, where the sample was heated from 25 to 220°C at a heating rate of 10°C min^{-1}, and then cooled from 220 to 25°C using different cooling rates (2.5, 5, 10, 20, and 40°C min^{-1}). The Kissinger and Avrami-Ozawa methods were used to determine the crystallization kinetics of the different crystalline phases.[15,16] Because the α- and β-crystals cocrystallize during the cooling process, the crystallization kinetics were evaluated for the combined crystallization.

A Perkin Elmer Spectrum 100 Fourier-transform infrared (FTIR) spectrometer was used to investigate whether an *in situ* chemical reaction occurred between the NAs at room temperature. It was particularly used to identify new bonds in the

Table II. Crystallization Peak Temperatures (T_c), and Melting Peak Temperatures of the β- and α- Polymorphs ($T_{\beta 1}$ and $T_{\alpha 1}$), in IPC

Sample	T_c (°C)	$T_{\beta 1}$ (°C)	$T_{\alpha 1}$ (°C)
Pristine IPC	120.1 ± 0.1		165.1 ± 0.8
IPC/Pim	127.2 ± 0.6	155.1 ± 0.4	166.8 ± 1.0
IPC/Pim-CaSt (1 : 2)	127.1 ± 0.3	155.3 ± 0.4	167.2 ± 1.0
IPC/Pim-CaSt (1 : 3)	127.0 ± 1.3	155.3 ± 1.7	167.3 ± 2.0
IPC/CaSt	120.9 ± 0.0	151.6 ± 0.2	165.7 ± 0.4
IPC/Adi	121.0 ± 0.1	152.6 ± 0.9	166.4 ± 0.4
IPC/Adi-CaSt (1 : 2)	122.2 ± 1.4	153.0 ± 1.5	166.5 ± 1.5
IPC/Adi-CaSt (1 : 3)	120.2 ± 1.1	150.7 ± 0.5	164.7 ± 0.5

bicomponent nucleants. The possibility of chemical interaction between the IPC and the nucleants was also investigated by FTIR. The samples were analyzed in an attenuated total reflectance (ATR) detector over a 400–4000 cm^{-1} wavenumber range at a resolution of 8 cm^{-1}.

A Bruker AXS D8 Advance X-ray diffractometer with filtered Cu-K_α radiation, and a PSD Vantec-1 gas detector with up to 1600 channels, was used to analyze the type and extent of crystallinity in the samples. The samples were scanned at 2θ angles between 10° and 50°, with a step size of 0.014°.

RESULTS AND DISCUSSION

The NE of the individual α and β NAs is shown in Figure 1. NE is dependent on both the molecular or crystal structure and the concentration and particle size of the NAs. To get a clear insight in the efficiency of NAs, the NE was estimated using the method developed by Fillon et al.[17] [eq. (1)].

$$\text{NE}\ (\%) = 100\frac{T_{cNA} - T_{c1}}{T_{c2max} - T_{c1}} \quad (1)$$

where T_{cNA}, T_{c1}, and T_{c2max} are the crystallization peak temperatures of the nucleated, non-nucleated, and self-nucleated polymer, respectively. Fillon et al.[17] approximated T_{c2max} by heating the sample to a temperature of 40°C above the melting temperature at a heating rate of 10°C min^{-1}. It was then held there for 10 min to erase all previous thermal history. The sample was then cooled to a temperature $T_1 = 50$°C at a cooling rate of 10°C min^{-1}. Thus, the crystallization will take place at the lower limit of the crystallization range (T_{c1}). The polymer was heated again until it was partially molten (melting temperature range). The secondary crystallization was followed by a subsequent cooling of the partially molten sample and the crystallization peak temperature is T_{c2} ($T_{c2} > T_{c1}$). The maximum crystallization peak temperature (T_{c2}) is denoted T_{c2max} ($T_{c2max} \sim 140$°C). The values of non-nucleated (T_{c1}) and nucleated (T_{cNA}) crystallization temperatures are shown in Table II. T_{c1} is the crystallization temperature of the pristine IPC, whereas T_{cNA} is that of the nucleated samples.

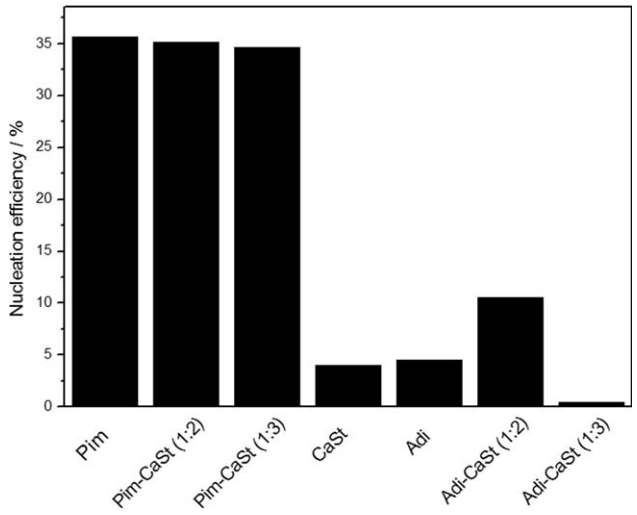

Figure 1. The nucleation efficiency of IPC nucleated with individual and compounded nucleating agents.

It can be clearly seen that pimelic acid (Pim) and its combination with calcium stearate (CaSt) have the highest NE of about 35%. This can be attributed to the perfect matching of the dimensional lattice between the c-axis of IPC and the corresponding distance in the crystal face of Pim.[18] It should, however, be realized that this is the efficiency of nucleation of all the crystal structures (only one DSC crystallization peak is observed—see Figures 4 and 5), and that the β-NE may be significantly higher, as was observed from the DSC and XRD results discussed below.

Calcium stearate (CaSt) and adipic acid (Adi), on the other hand, have low NE values of about 5%. Pim and its combination with CaSt cause an increase in T_c of iPP, whereas Adi, CaSt, and their combination have very little effect on T_c. The high NE value for IPC-Pim suggests that the NE of Pim will not be significantly affected when compounded with CaSt. As can be seen in Figure 1, there is only a slight decrease in NE when Pim is compounded with CaSt. It is clear that the calcium pimelate, which forms when Pim is compounded with CaSt (see FTIR discussion below), is equally efficient as NA. Adi and CaSt have low NE values, but the calcium adipate, formed when compounding Adi and CaSt in a 1 : 2 mass ratio, has an observably better NE. When compounded in a 1 : 3 mass ratio, the product has a much lower NE than both Adi and CaSt. It is not clear why there is such a big difference in nucleation efficiencies of the two Adi-CaSt combinations. One reason may be experimental errors in the determination of the crystallization peak temperatures. As can be seen from Table II, the standard deviation on the T_c value for IPC/Adi-CaSt (1 : 2) is quite big. Another reason may be that for the Adi-CaSt (1 : 2) not all the Adi has reacted with CaSt (the molar ratio is about 2 : 1) and that the combination of the unreacted Adi and the calcium adipate is a more effective NA than Adi-CaSt (1 : 3), which will contain less unreacted Adi.

The first heating curves of all the IPC samples nucleated with the individual and compounded NAs are shown in Figures 2 and 3. Both figures show three distinctive peaks where the small peak at about 115°C is attributed to the melting peak of the crystallizable polyethylene (PE) segments present in IPC. This peak can be seen in both the pure and nucleated samples. It is

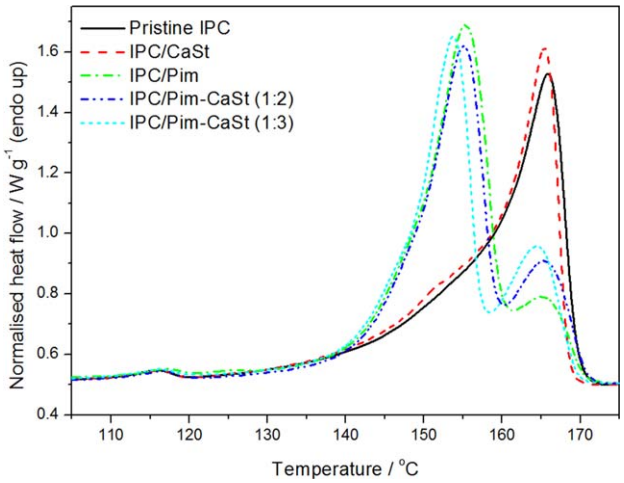

Figure 2. DSC heating curves of IPC nucleated with individual (Pim, CaSt) and compounded nucleants. [Color figure can be viewed in the online issue, which is available at wileyonlinelibrary.com.]

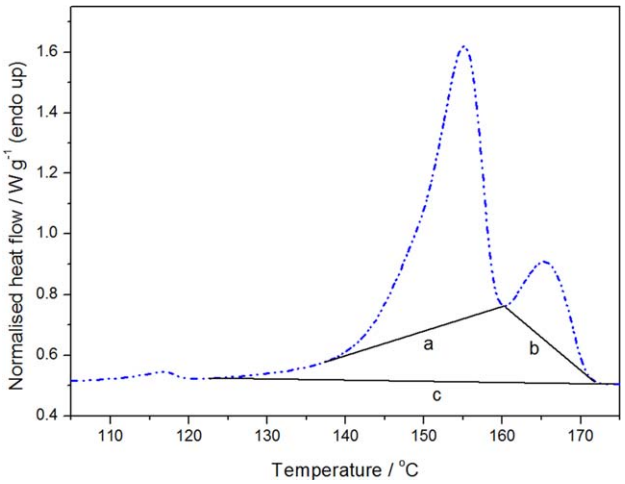

Figure 4. Illustration of how the overlapping melting peaks in the DSC curves were resolved. [Color figure can be viewed in the online issue, which is available at wileyonlinelibrary.com.]

clear that the addition of NAs did not change the melting profile of these segments. There is also a peak at about 155°C in Figure 2, which is ascribed to the melting of the β-crystals. This peak can also be seen around 150°C in Figure 3. Another melting peak is observed around 165°C and it is attributed to the melting of the α-crystals.[19]

It is worth noting that all the investigated NAs induced β-crystals in IPC, even though their efficiency differed. In Figure 2, the β-crystal melting peak is only pronounced in IPC/Pim, IPC/Pim-CaSt (1 : 2), and IPC/Pim-CaSt (1 : 3), whereas in IPC/CaSt it is almost negligibly small. Figure 3 shows that the β-crystal melting peak is more resolved but still small for the IPC/Adi-CaSt (1.2) and IPC/Adi-CaSt (1 : 3) samples. Pim alone is, therefore, a very efficient and selective β-nucleant. The compounding of Pim and CaSt could not further improve the effectiveness of β-nucleation in IPC, and the presence of CaSt also did not significantly improve the poor nucleating efficiency of Adi.

An increase in the Adi-CaSt ratio increases the melting enthalpy of the α-crystals (Table III). The calcium adipate seems to have a dual activity to enhance both α- and β-crystal formation, but it has a lower efficiency to induce β-crystal formation. The β-crystal peak is, however, much better resolved and more intense than those of IPC-Adi and IPC-CaSt, although not nearly as strong as in the case of Pim and Pim-CaSt. As the amount of CaSt increases in Adi-CaSt, the intensity of the β-crystal peak decreases slightly, whereas that of the α-crystal increases. This confirms that the presence of primarily calcium adipate has a stronger ability for α-crystal formation. It can be seen from Table II that the melting peak temperatures of the α- and β-phases are very similar within experimental error for all the samples. The small differences observed may be related to

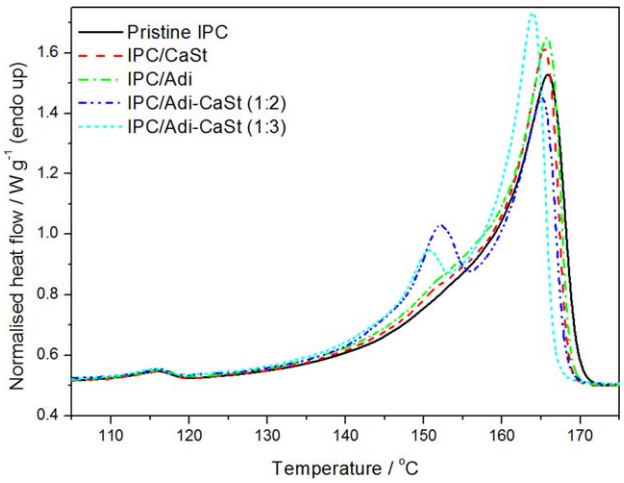

Figure 3. DSC heating curves of IPC nucleated with individual (Adi, CaSt) and compounded nucleants. [Color figure can be viewed in the online issue, which is available at wileyonlinelibrary.com.]

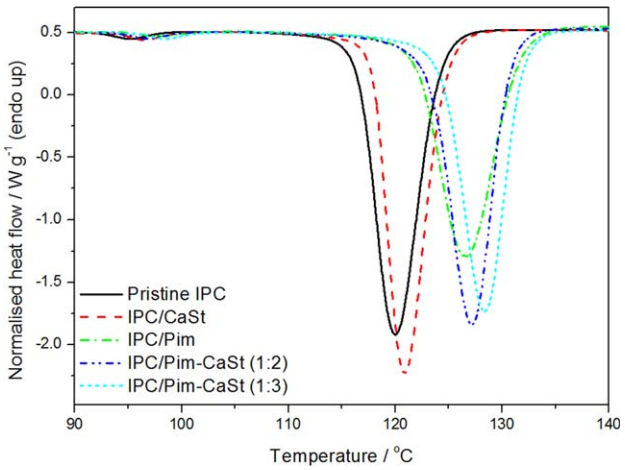

Figure 5. DSC cooling curves of IPC nucleated with individual (Pim, CaSt) and compounded nucleants. [Color figure can be viewed in the online issue, which is available at wileyonlinelibrary.com.]

Table III. Summary of the DSC Melting and Crystallization Results of the Investigated Samples

Sample	$\Delta H_{m,\beta}$ (J g^{-1})	$\Delta H_{m,\alpha}$ (J g^{-1})	K_{DSC} (%)	X_{DSC} (%)
Pristine IPC		77.2 ± 0.1		43.6
IPC/Pim	60.8 ± 1.7	10.8 ± 1.4	85.5 ± 1.9	30.6
IPC/Pim-CaSt (1 : 2)	65.4 ± 1.9	8.7 ± 1.6	88.8 ± 2.1	43.7
IPC/Pim-CaSt (1 : 3)	65.3 ± 0.5	9.8 ± 1.1	87.5 ± 1.1	44.3
IPC/CaSt	0.4 ± 0.0	61.4 ± 1.5	0.6 ± 0.0	34.9
IPC/Adi	3.0 ± 0.0	60.3 ± 0.0	10.0 ± 0.0	17.9
IPC/Adi-CaSt (1 : 2)	11.6 ± 0.0	58.9 ± 1.2	17.1 ± 0.3	40.2
IPC/Adi-CaSt (1 : 3)	5.0 ± 0.4	70.4 ± 1.6	6.9 ± 0.7	42.7

$\Delta H_{m,\beta}$ and $\Delta H_{m,\alpha}$ are the melting enthalpies of the β- and α-crystals; K_{DSC} and X_{DSC} are the calculated amount of β-content and total crystallinity.

crystal sizes and size distributions, which will be due to differences in effectiveness of crystal growth.

The DSC cooling curves of the virgin and nucleated samples are shown in Figures 4 and 5. The melting enthalpies of the α- and β-crystals, the β-crystal fractions, and the total crystallinities are tabulated in Table III. The β-contents for all the samples were calculated using eq. (2).

$$K_{DSC}(\%) = \frac{X_\beta}{X_\beta + X_\alpha} \quad (2)$$

where X_β and X_α are the crystallinity values of the β- and α-crystals, respectively. The respective crystallinities of the α- and β-phases were calculated from the average enthalpy values by using eq. (3), after manually resolving the slightly overlapping melting peaks. The individual resolved enthalpies were calculated by separately determining the enthalpies of the peaks having baseline a (melting of β-crystals: ΔH_a) and baseline b (melting of α-crystals: ΔH_b), as well as that of the combined overlapping peaks having baseline c (ΔH_c) in Figure 4. Each resolved enthalpy was then calculated by using eq. (4).

$$X(\%) = \frac{\Delta H_m}{\Delta H_m^\circ} \times w_{IPC} \quad (3)$$

where ($\Delta H_m \times w_{IPC}$) is the normalized melting enthalpy and ΔH_m° is the melting enthalpy of the pure crystalline PP. The ΔH_m° values for the β- and α-crystals were taken as 168.5 J g^{-1} and 177 J g^{-1}, respectively.[20] The total crystallinity, X_{DSC}, is the sum of the α- and β-crystallinities in each case.

$$\Delta H_{a,res} = [\Delta H_c/(\Delta H_a + \Delta H_b)] \times \Delta H_a \quad (4)$$

where $\Delta H_{a,res}$ is the enthalpy for the resolved β-crystal melting peak. The enthalpy for the resolved α-crystal melting peak was calculated in the same way from ΔH_b.

Figures 5 and 6 show two crystallization peaks for all the investigated samples. The first peak appearing around 95°C is ascribed

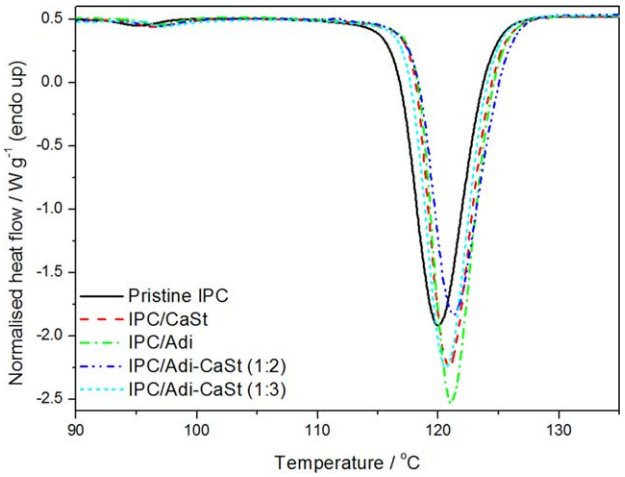

Figure 6. DSC cooling curves of IPC nucleated with individual (Adi, CaSt) and compounded nucleants. [Color figure can be viewed in the online issue, which is available at wileyonlinelibrary.com.]

to the crystallization of the PE segments in IPC. The crystallization peak at higher temperatures is ascribed to the crystallization of both the α- and β-crystals. The presence of different NAs gives rise to crystallization at different temperatures. The presence of CaSt alone in IPC slightly increases T_c, whereas Pim and Pim-CaSt significantly increase this value. This can be explained by the good nucleation activity of Pim. There is very little difference between the T_c values of IPC and its samples nucleated with Adi, CaSt, and Adi-CaSt. This is in line with the already discussed low nucleating efficiency of these NAs.

Figure 7 shows the FTIR spectra of the individual and compounded NAs dissolved in acetone at room temperature, and dried overnight. For simplicity of the discussion the observed frequency bands are divided into two sets: aliphatic (methylene and methyl) and carboxyl groups (COOH). Both pimelic and adipic acid show weak absorption peaks around 2955 cm^{-1}, whereas CaSt and the compounded nucleants shows very strong double peaks at about the same absorption wavenumbers. The vibration bands are associated with the aliphatic groups present in the NAs. The peak at higher frequency is associated with the C—H stretching of CH_3, whereas that at lower frequency is ascribed to the C—H stretching of CH_2.[21,22] It is accepted that, in CaSt, the calcium metal is sandwiched by carbonyl functional groups, accompanied by moderately long alkyl chains.[23] The dicarboxylic acids, however, have fairly short methylene chains (five and four methylene groups respectively situated between the carbonyl groups in Pim and Adi). This explains the low peak intensities of these peaks in Pim and Adi. Both the dicarboxylic acids show a discernible peak band around 1698 cm^{-1}, which is attributed to as the C═O stretching mode of —COOH, and which is not observed in CaSt. The two peaks at 1193 and 1278 cm^{-1} in the spectra of Pim and Adi are associated with the stretching mode of the C—O bond in the diacids.[21] The compounded nucleants show only one peak in this wavenumber range, which could be the result of a chemical reaction which occurred between CaSt and the diacids. Evidence from other techniques (not available in our laboratory) will, however, be

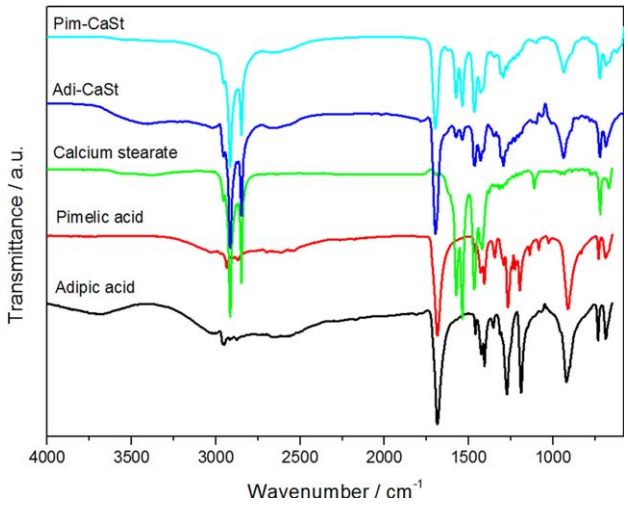

Figure 7. FTIR spectra of individual and compounded nucleating agents. [Color figure can be viewed in the online issue, which is available at wileyonlinelibrary.com.]

needed to confirm such a reaction. The peaks at 1578 and 1546 cm^{-1} in CaSt (not seen in the spectra of the diacids) have been assigned to the COO^- stretching vibration of carboxylate groups in unidendate and bidendate coordination with calcium ions, respectively.[24] These vibrations are also visible in the compounded nucleants' spectra, which is probably the result of unreacted calcium stearate in the respective systems.

The FTIR spectra of IPC and the nucleated samples are presented in Figure 8. Two peaks at about 1577 and 1750 cm^{-1} are observed in the nucleated samples. These peaks are either not observed in the spectrum of IPC, or they are much less intense. These peaks are associated with the COO^- stretching vibration of —COOH, and the C=O stretching mode of the carbonyl group. The intensities of these vibrations are higher and they are shifted to higher wavenumbers. This can be attributed to the molecular rearrangement in forming the β-polymorph in

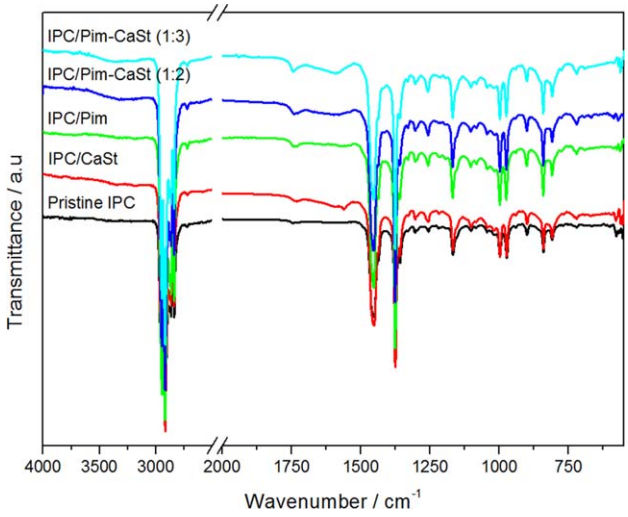

Figure 8. FTIR spectra of IPC samples prepared in the absence and presence of individual and compounded Pim and CaSt. [Color figure can be viewed in the online issue, which is available at wileyonlinelibrary.com.]

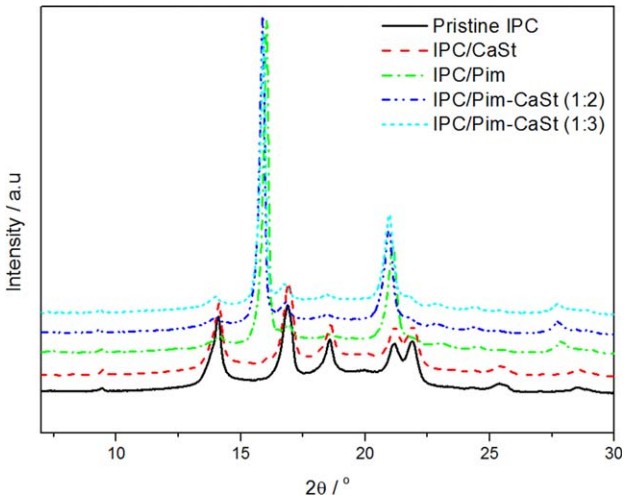

Figure 9. XRD spectra of non-nucleated and nucleated IPC with individual (Pim, CaSt) and compounded nucleants. [Color figure can be viewed in the online issue, which is available at wileyonlinelibrary.com.]

IPC.[25] The peak in the 670–750 cm^{-1} range, which is assigned to the methyl rocking —$(CH_2)_n$— vibration, becomes more pronounced for the nucleated samples, which indicates the presence of the different NAs on the surface of IPC.[26] Because the antioxidant shows only one low-intensity peak at 845 cm^{-1}, it had no influence on the FTIR spectra. The IPC matrix has a hydrophobic character, whereas all the NAs have both hydrophobic and hydrophilic characters. Thus, the IPC chains interact better with the nonpolar part of the NAs. This phenomenon drives the IPC chains to create stable β-nuclei. The NAs create certain spatial sites for IPC nucleation, eventhough there is a barely observed chemical interaction between them. It is also clear that the system used in this work does not change the chemical structure of IPC.

The β-content in the nucleated samples was calculated using the Turner-Jones equation[27] [eq. (5)].

$$K_{XRD} = \frac{A_\beta(300)}{A_\beta(300)+A_\alpha(110)+A_\alpha(040)+A_\alpha(130)} \quad (5)$$

where $A_\beta(300)$ is the area under the (300) reflection peak, and $A_\alpha(110)$, $A_\alpha(040)$, and $A_\alpha(130)$ are the areas under the (110), (040), and (130) reflection peaks, respectively. The peaks are at 16.1° for $A_\beta(300)$, and 14.1°, 16.9°, and 18.8° for the $A_\alpha(110)$, $A_\alpha(040)$, and $A_\alpha(130)$ on the spectrum. The total crystallinity of all the samples was calculated by using eq. (6).

$$X_{XRD} = \frac{\sum A_{cryst}}{\sum A_{cryst} + \sum A_{amorp}} \quad (6)$$

where A_{cryst} and A_{amorp} are the fitted areas of the crystal and amorphous domains, respectively.

The XRD spectra of all the samples are shown in Figures 9 and 10. The peaks that are more prominent for the α- and β-polymorphs are used in eq. (4). Generally, the formation of

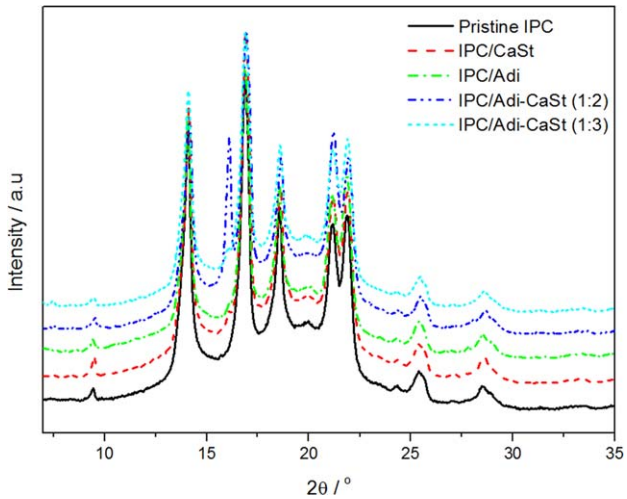

Figure 10. XRD spectra of non-nucleated and nucleated IPC with individual (Adi, CaSt) and compounded nucleants. [Color figure can be viewed in the online issue, which is available at wileyonlinelibrary.com.]

β-crystals is seen in all the nucleated samples. Because Pim has a good NE, the strong α-peaks of the lattice coordinates (040) and (130) decreased considerably. Even where the Pim is compounded with CaSt at various ratios there is also a decrease in the intensity of these peaks. When Adi is compounded with CaSt in a 1 : 2 ratio, the development of the β-crystal peak can be seen, which shows that calcium adipate is a more efficient NA than the individual NAs.

Table IV summarizes the XRD peak areas and the calculated crystallinities and β-contents. It can be seen that the β-contents of the Pim and Pim-CaSt nucleated samples are virtually the same, and the values are in line with the values obtained from the DSC melting peaks (Table II). Adding CaSt, as well as an increase in the amount of CaSt, obviously does not have a significant impact on the formation of β-crystals. This can be attributed to the high NE of Pim. The total crystallinity for pristine IPC, determined from XRD, is slightly lower than that determined from the DSC melting peaks, but the total crystallinities for the nucleated samples are much higher. The reason for this is probably that the crystals, formed as a result of nucleation in the presence of Pim, are thermally labile and that "decrystallization" takes place during the heating process in the DSC. For the Adi and Adi-CaSt samples, both the β-content and crystallinities correlate well with those determined from the DSC curves.

The nonisothermal crystallization kinetics was evaluated by using the Ozawa and Avrami-Ozawa equations.[28] The crystallization activation energy values were determined through Kissinger's method [eq. (7)].[29]

$$\frac{d\ln\left(\varphi/T_c^2\right)}{d(1/T_c)} = \frac{-\Delta E}{R} \tag{7}$$

where T_{cp}, ΔE, R, and φ are, respectively, the crystallization temperature, activation energy, gas constant, and the cooling rate. This equation can be evaluated and be rewritten [eq. (8)].

$$\ln\left(\frac{\varphi}{T_c^2}\right) = \frac{-\Delta E}{R}\left(\frac{1}{T_c}\right) + C \tag{8}$$

The crystallization activation energy is determined from the slope of the linear plot of $\ln(\varphi/T_c^2)$ against $1/T_c$. Equation 8 is the well-known Avrami equation for isothermal kinetics analysis. The general form of the Avrami equation is given by eq. (9).

$$X_t = 1 - \exp\left(-Z_t t^n\right) \tag{9}$$

where X_t is the relative crystallinity at time t, n is the Avrami parameter which depends on the nucleation mechanism, and Z_t is a constant which describes the nucleation and growth parameters. At constant temperature, eq. (9) can be modified to give eq. (10).

$$\ln\left(-\ln\left(1-X_t\right)\right) = \ln Z_t + n\ln t \tag{10}$$

Ozawa considered the effect of cooling rate and the Avrami equation was adapted to eq. (11).

$$X_t = 1 - \exp\left(-\frac{K(T)}{\varphi^m}\right) \tag{11}$$

where X_t is the relative crystallinity at time t, m is the Ozawa parameter which also depends on the nucleation mechanism,

Table IV. Summary of the XRD Crystalline Phase Parameters of the Investigated Samples

Sample	A_α (110) ~ 14.1°	A_α (040) ~ 16.9°	A_α (130) ~ 18.8°	A_β (300) ~ 16.1°	K_{XRD} (%)	X_{XRD} (%)
Pristine IPC	11588	10873	4175			32
IPC/Pim	1455	716	957	27254	90	70
IPC/Pim-CaSt (1 : 2)	1393	984	719	25323	89	80
IPC/Pim-CaSt (1 : 3)	1103	1165	672	24078	89	78
IPC/CaSt	11690	11734	4438			16
IPC/Adi	10052	9469	4021			21
IPC/Adi-CaSt (1 : 2)	8078	8360	3962	2742	12	27
IPC/Adi-CaSt (1 : 3)	10330	10038	4149			29

A_α (110), A_α (040), A_α (130) and A_β (300) are peak areas of the alpha and beta crystals at reflection lattice planes of (110), (040), (130), and (300), respectively. K_{XRD} and X_{XRD} are the amount of β-crystals and the total crystallinity calculated using XRD.

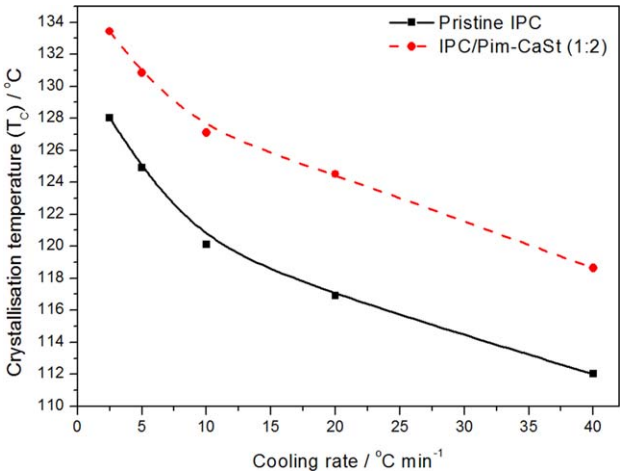

Figure 11. crystallization peak temperatures of pure and nucleated IPC at different cooling rates. [Color figure can be viewed in the online issue, which is available at wileyonlinelibrary.com.]

and $K(T)$ is the crystallization rate constant. Equation (10) can be rearranged into eq. (12).

$$\ln(-\ln(1-X_t)) = \ln K(T) - m\ln\varphi \tag{12}$$

The relationship between the temperature and crystallization time can be described by eq. (13).

$$t = \frac{T_0 - T}{\varphi} \tag{13}$$

where T is the temperature at time t, T_o is the temperature at the start of the crystallization process. Since the degree of crystallinity is related to the cooling rate φ and the crystallization time t, combination of eqs. (9) and (11) gives eq. (14).

$$\ln Z_t + n\ln t = \ln K(T) - m\ln\varphi \tag{14}$$

which may be rearranged to give eq. (15).

$$\ln\varphi = \ln F(T) - a\ln t \tag{15}$$

where $F(T) = \{K(T)/Z_t\}^{1/m}$ refers to the cooling rate value, which has to be chosen at unit crystallization time when the measured system amounts to a certain degree of crystallinity. According to Liu et al.[30] $F(T)$ has a definite physical and practical meaning, but it is not clear from the rest of their discussion exactly what this meaning is. The parameter a is the ratio of the Avrami exponent n to the Ozawa exponent m ($a = n/m$).

To investigate the crystallization kinetics, the samples were cooled from the molten state at different cooling rates (2.5 to 40°C min^{-1}). We used cooling rates lower than 50°C min^{-1} because it has been found[31] that β-crystals only form on cooling the melt at rates lower than 50°C min^{-1}. It is evident that T_c decreases with an increase in cooling rate (Figure 11). This is in line with the results reported in previous studies,[15,30] and it is because crystallization is a kinetic time-dependent process. The pristine IPC has lower T_c values than the nucleated IPC sample. The presence of compounded NAs, because of their nucleation effect, causes the IPC crystallization to start at higher temperatures.

Table V. Crystallization Half-Life ($t_{1/2}$) at Different Cooling Rates for Neat and Nucleated IPC

Pristine IPC					
Cooling rate (°C min^{-1})	2.5	5	10	20	40
$T_{1/2}$ (min)	2.2	1.4	0.8	0.4	0.3
IPC/Pim-CaSt (1 : 2)					
Cooling rate (°C min^{-1})	2.5	5	10	20	40
$T_{1/2}$ (min)	2.2	1.2	0.8	0.4	0.2

The relative crystallinity for each investigated sample is shown as a function of crystallization temperature by eq. (16).

$$X_t = \frac{\int_{T_o}^{T}(dH_c/dT)dT}{\int_{T_o}^{T_\infty}(dH_c/dT)dT} \tag{16}$$

where T_o and T_∞ are the onset and end of crystallization temperatures, and dH_c/dT is the rate of heat evolution at temperature T. The crystallization half-life was determined from the sigmoidal curves described by eq. (16) as the time at 50% relative crystallinity and are tabulated in Table V for the different cooling rates. The crystallization half-lives of the pristine IPC and IPC/Pim-CaSt (1 : 2) are virtually the same at the same cooling rates. It seems as if the NA did not significantly influence the crystallization rate of the IPC, although the crystallization in this case started at higher temperatures. Other authors found that the crystallization half-life slightly decreased in nucleated samples when compared to that of the pure material at the same cooling rate.[15] The Ozawa parameters (m) of the samples were obtained from the slope of the linear Ozawa plots according to eq. (14), and are tabulated in Table VI. The average values of 2.8 and 3.0 indicate that the crystallization mode is a three-dimensional growth with athermal nucleation mechanism.[32] It seems as if the nucleation mechanism did not change with the addition of Pim-CaSt (1 : 2). The a ($= n/m$) values in Table VI were estimated from the slope of the Avrami-Ozawa linear plots [eq. (15)], where n and m are the Avrami and Ozawa exponents. The fact that $a \neq 1$ is probably because of secondary crystallization, although it is difficult to establish the real meaning of a from the available literature. It is, however, interesting to see that the value of a did not change significantly for the β-nucleated sample, which further confirms that the nucleation mechanism is similar for α- and β-nucleation. The

Table VI. Nonisothermal Crystallization Kinetics Parameters Determined by the Ozawa-Avrami and Kissinger Methods

	A	m	ΔE (kJ mol^{-1})
Pristine IPC	1.3	2.8	230
IPC/Pim-CaSt (1 : 2)	1.2	3.0	255

crystallization activation energy (ΔE) is slightly lower for the pristine IPC, which confirms that the α- crystallization is the thermodynamically preferred process.

CONCLUSIONS

The aim of this work was (i) to induce the highest possible β-crystal content in an IPC by adding NAs and also by using a feasible preparation method, (ii) to establish the NE of the individual and bicomponent nucleants, and (iii) to investigate the crystallization behavior and kinetics of IPC.

Nucleated IPC samples were prepared by extrusion followed by compression moulding under preinvestigated conditions that were found to induce the highest β-crystal content. When using pimelic acid based NAs, we managed to obtain samples with about 90% of β-crystals. However, calcium stearate and adipic acid based NAs had very low NE values, and correspondingly gave rise to very low or no β-crystal contents. Generally, the combination of pimelic acid and adipic acid with calcium stearate did not significantly change the NEs of the respective acids, although the Adi-CaSt (1 : 2) combination seemed to have given slightly better results. None of the NAs chemically reacted with IPC, and the chemical structure of the polymer was thus intact during the treatment.

Investigation of the crystallinities of the different nucleated samples showed higher total crystallinity values for the Pim nucleated samples from the XRD measurements than from the DSC measurements. This was attributed to the fact that the crystals, formed as a result of nucleation in the presence of Pim, were thermally labile and that "decrystallization" took place during the heating process in the DSC. The α- and β-crystallization were found to occur over the same temperature range, and nonisothermal crystallization kinetics revealed the crystallization to occur according to a three-dimensional growth with athermal nucleation mechanism. The treatment with NAs did not seem to change the crystallization mechanism of IPC, although it was found that α-crystallization is the thermodynamically preferable process because of the low crystallization activation energy of non-nucleated IPC.

ACKNOWLEDGMENTS

The National Research Foundation of South Africa, and the Universities of the Free State and Stellenbosch are acknowledged for financial support of the project.

REFERENCES

1. Menyhard, A.; Varga, J.; Molnar, G. *J. Therm. Anal. Calor.* **2006**, *83*, 625.
2. Li, X.; Wu, H.; Huang, T.; Shi, Y.; Wang, Y.; Xiang, F.; Zhou, Z. *Colloid Polym. Sci.* **2010**, *288*, 1539.
3. Xiao, W.; Wu, P.; Feng, J.; Yao, R. *J. Appl. Polym. Sci.* **2009**, *111*, 1076.
4. Li, J. X.; Cheung, W. L. *J. Vinyl Addit. Technol.* **1997**, *3*, 151.
5. Krache, R.; Benavente, R.; Lopez-Majada, J. M.; Perena, J. M.; Cerrada, M. L.; Perez, E. *Macromalecules* **2007**, *40*, 6871.
6. Zhang, P.; Liu, X.; Li, Y. *Mater. Sci. Eng.* **2006**, *434*, 310.
7. Menyhard, A.; Varga, J.; Liber, A.; Belina, G. *Eur. Polym. J.* **2005**, *41*, 669.
8. Liu, T.; Meng, H.; Liu, T.; Sheng, X.; Zhang, X. *Polym.-Plast. Technol. Eng.* **2011**, *50*, 1165.
9. Mahdavi, H.; Nook, M. E. *Polym. Int.* **2010**, *59*, 1701.
10. Zhang, R. H.; Shi, D.; Tjong, S. C.; Li, R. K. Y. *J. Polym. Sci. Part B: Polym. Phys.* **2007**, *45*, 2674.
11. Yang, Z.; Mai, K. *J. Appl. Polym. Sci.* **2011**, *119*, 3566.
12. Yang, Z.; Mai, K. *Thermochim. Acta* **2010**, *511*, 152.
13. Grein, C.; Gahleiner, M. *Exp. Polym. Lett.* **2008**, *2*, 392.
14. Luo, F.; Xu, C.; Ning, N.; Wang, K.; Deng, H.; Chen, F.; Fu, Q. *Polym. Int.* **2013**, *62*, 172.
15. Xui, L.; Zhang, X.; Xu, K.; Lin, S.; Chen, M. *Polym. Int.* **2010**, *59*, 1441.
16. Wang, J.; Dou, Q. *J. Macromol. Sci. Part B: Phys.* **2008**, *47*, 629.
17. Fillon, B.; Thierry, A.; Lotz, B.; Wittmann, J. C. *J. Therm. Anal.* **1994**, *42*, 721.
18. Zeng, A.; Zheng, Y.; Qui, S.; Guo, Y.; Li, B. *Colloid Polym. Sci.* **2011**, *289*, 1157.
19. Wei, Z.; Zhang, W.; Chen, G.; Liang, J.; Yang, S.; Wang, P.; Liu, L. *J. Therm. Anal. Calor.* **2010**, *102*, 775.
20. Luo, F.; Wang, K.; Ning, N.; Geng, C.; Deng, H.; Chen, F.; Fu, Q.; Qian, Y.; Zheng, D. *Polym. Adv. Technol.* **2011**, *22*, 2044.
21. Kagarise, R. E. *J. Phys. Chem.* **1955**, *59*, 271.
22. Colthup, N. B. *J. Opt. Soc. Am.* **1950**, *40*, 397.
23. Gonen, M.; Ozturk, S.; Balkose, D.; Okur, S.; Ulku, S. *Ind. Eng. Chem. Res.* **2010**, *49*, 1732.
24. Lu, Y.; Miller, J. D. *J. Colloid Interface Sci.* **2002**, *256*, 41.
25. Lorenzo, V.; Polo-Corpa, M. J.; Perez, E.; Benavente, R.; de la Orden, M. U.; Martınez-Urreaga, J. *J. Appl. Polym. Sci.* **2011**, *121*, 1023.
26. Li, X.; Hu, K.; Ji, M.; Huang, Y.; Zhou, G. *J. Appl. Polym. Sci.* **2002**, *86*, 633.
27. Turner-Jones, A.; Aizlewood, J. M.; Beckett, D. R. *Die Makromol. Chem.* **1964**, *75*, 134.
28. Ozawa, T. *Polymer* **1971**, *12*, 150.
29. Kissinger, H. E. *J. Res. Natl. Bur Stand.* **1956**, *57*, 217.
30. Liu, T.; Mo, Z.; Wang, S.; Zhang, H. *Polym. Eng. Sci.* **1997**, *37*, 568.
31. Mollova, A.; Androsch, R.; Mileva, D.; Gahleitner, M.; Funari, S. S. *Eur. Polym. J.* **2013**, *49*, 1057.
32. Jiang, X. L.; Luo, S. J.; Sun, K.; Chen, X. D. eXPRESS Polym. *Lett.* **2007**, *1*, 245.